Clays Clay Miner., Vol. 70, No. 5:601–615, 2022
https://doi.org/10.1007/s42860-022-00208-2

ORIGINAL PAPER

Influence of Thermal Treatment of Moroccan Red Clay on its Physicochemical and Mechanical Behavior

M. A. Harech · T. Labbilta · Y. Abouliatim · Y. Elhafiane · A. Benhammou · A. Abourriche · A. Smith · L. Nibou · M. Mesnaoui

Accepted: 7 October 2022 / Published online: 10 November 2022

Abstract Red clay is considered to be of significant value to the economy in Morocco, particularly in the Safi region, because of its abundance. This raw material has long been known for its quality in the manufacture of clay materials, but its use was limited to traditional ceramics. The red clay raw material was the subject of the current study with the objective of opening new industrial applications that will give added value to the Safi red clay. The physicochemical, mineralogical, and thermal properties of the Moroccan red clay were determined by X-ray fluorescence (XRF), inductively coupled plasma-atomic emission spectroscopy (ICP-AES) analysis, X-ray diffraction (XRD), oriented aggregate, and particle-size analyses, powder density by helium pycnometry, carbonate content using the Bernard method, differential thermal analysis (TG–DTA), and the BET surface area. The compacted dry powder particles were calcined at three sintering temperatures: 900, 1000, and 1100°C for 2 h. The effect of sintering temperature on ceramic properties, such as apparent porosity, water adsorption, bulk density, and mechanical strength, was examined. Dense ceramics with lower porosity and greater mechanical resistance (~300%) were produced by increasing the sintering temperature from 900 to 1100°C. The conclusion was that the evolution of physicochemical and thermal properties is related to mineralogical changes, which show that anorthite is the major phase at higher temperatures.

Keywords Ceramic · Clay · Thermal treatment · Mineralogical transformations

Associate Editor: Chun Hui Zhou.

M. A. Harech (✉) · T. Labbilta · M. Mesnaoui
Laboratory of Materials Sciences and Processes Optimization, Chemistry of Condensed Matter and Environment Team, Chemistry Department, Faculty of Sciences Semlalia, Cadi Ayyad University, 40000 Marrakech, Morocco
e-mail: mharech@gmail.com

Y. Abouliatim · A. Benhammou · A. Abourriche · L. Nibou
Laboratory of Materials, Processes, Environment, and Quality, National School of Applied Sciences of Safi, Cadi Ayyad University, 46000 Safi, Morocco

Y. Elhafiane · A. Smith
Institut de Recherche Sur Les Céramiques, IRCER - UMR 7315, Université de Limoges, Centre Européen de La Céramique, 12 rue Atlantis, 87068 Limoges Cedex, France

M. Mesnaoui
Center of Excellence in Soil and Fertilizer Research in Africa (CESFRA), AgroBioSciences, Mohammed VI Polytechnic University, 43150 Ben Guerir, Morocco

Introduction

Clay is the material which has been used longest by humankind, and it is essential in the manufacture of objects used in daily life. Clay is undergoing a renaissance in the construction, industrial ceramics, artisanal, pharmaceutical, and pottery sectors (Kabre et al.,

1998; Strazzera et al., 1997). The most common types of ceramics are made from clay-based materials. They consist usually of complex natural mixtures of minerals with highly diverse grain sizes and physicochemical properties (Celik, 2010; Njoya et al., 2012). The quality of the resulting ceramic product depends on several parameters, related mainly to the nature of the basic raw materials used and the behavior throughout the manufacturing steps of the ceramic products. Thus, the ceramic products can be refined at two levels: firstly, the quality of the chosen raw materials; and secondly, the manufacturing process (preparation of the paste, shaping, drying techniques, type of firing, and enameling). Most ceramic products are obtained through sintering, generally between 900 and 1200°C. The sintering process is linked to the composition of the raw material and it is coupled with microstructural transformations of the initial minerals as a function of temperature and firing time (Djangang et al., 2008; Harech et al., 2019; Monteiro & Vieira, 2004). These materials undergo physicochemical transformations that lead to both a modification of the crystalline structure at the various stages (dehydroxylation, amorphization, crystallization, transformation, decarbonization, etc.) and a modification of the microstructure of the mixture (distribution and orientation of pores, coarsening of grains or crystals, etc.). These transformations are accompanied by changes in the mechanical properties (Jordan et al., 2008). This parameter is essential because the usage properties of many ceramic materials made from clay are often linked to their mechanical resistance under compression (bricks, sanitaryware, etc.) or bending (tiles, wall tiles, dishes). The investigation and monitoring of the sintering process are essential to determine the optimal temperature to achieve the desired degree of densification. Currently, with the increase in the price of energy, the trend among ceramists is to reduce the duration and temperature of the sintering of products to a bare minimum. In Morocco, clay is used mainly to produce traditional and modern building materials (bricks, tiles, sanitary ware) and to manufacture many ceramic products. Morocco has sufficient clay resources to ensure all or part of the supply of the ceramics industry. Previous work has identified important clay fields in Morocco; these include the three main regions of the country, namely Safi, Salé, and Fès-Meknès (El Ouahabi, 2013). Safi clay forms a vital catchment area, which forms the foundation of Safi city and is used to make pottery. The exploitation of clay in the ceramics industry is generally artisanal and semi-industrial in Morocco, and these activities are established and managed by family-owned companies and artisans. The lack of previous studies and the resulting dearth of knowledge about the properties and behavior of the red clay accounts for many of the problems which occur during production, including fractures and misshapen or deformed final products. Such problems limit productivity significantly. To date, no study has been reported on the thermal behavior of Safi clay, which is frequently used as a raw material in many studies, without focusing on its thermal behavior. The current study aimed to evaluate the effect of temperature on the thermal behavior of Safi clay and to provide new data on its mineralogical, physicochemical, thermal, and mechanical changes due to temperature increases. These data will help in the future manufacture of value-added ceramics. Results from this study are expected to contribute further knowledge and more in-depth characterization of clay in Morocco and, more precisely, the red clay of the Safi region. The specific objectives of the present research were:

- to study the red clays of the Safi region to extend the data which serve as a foundation for start-up projects for the industrial use of local clay materials and other research; and
- to characterize red clay as a raw material used by artisans and ceramists and its suitability for the production of mass-market ceramic products.

Materials and Methods

Sample Elaboration

The raw material used in this study was obtained from Al Barrage (Morocco, Safi region, coordinates 32.324962, -9.188877). First, the clay was dried in an electric oven at 105°C for 24 h and then milled. After grinding, the powder was sieved to a size of <100 µm. The pellets were prepared from red clay by a dry method. The powder was compressed axially under a load of 1 ton to obtain pellets with a diameter of 13 mm and a thickness of 3 mm, then heated to various temperatures. The heat treatment was carried out in an electric furnace (LH 15/12 System, Nabertherm,

https://doi.org/10.1007/s42860-022-00208-2 Published online by Cambridge University Press

Lilienthal, Germany) according to the following thermal cycle:

Increase the temperature to the selected cooking temperature (600, 900, 1000, or 1100°C) at a rate of 5°C/min; followed by 2 h dwell time at the selected temperature and natural cooling with the furnace turned off.

Analytical Techniques

An XRF analysis was performed to identify the chemical composition and predict the mineralogy of the analyzed sample. A Panalytical ZETIUM X-ray fluorescence instrument (Malvern Panalytical, Malvern, UK) was used to analyze for major and trace elements. The red clay was ground finely in an agate mortar before analysis. Then 1 g of the dried sample was mixed with 10 g of lithium tetraborate (Sigma-Aldrich, St Louis, Missouri, USA). The resulting mixture was fired to 1065°C, melted in a platinum crucible, and then molded into a glass disk. The characterization of the mineral phases in the raw material and the ceramics fired at 600, 900, 1000, and 1100°C was carried out by XRD (Malvern Panalytical, Malvern, UK) using the powder method. Samples were milled in an agate mortar to a fine powder (<100 μm). A diffractometer from Rigaku SmartLab (Tokyo, Japan) was used, and the data were collected over a range of 5 to 55°2θ with a step size of 0.04°2θ, using CuKα radiation (λ = 1.5405 Å). Mineral identification was carried out by matching the ICDD 2016 database lines to the diffraction peaks.

Inductively coupled plasma optical emission spectroscopy (ICP-AES, Ultima Expert, Horiba Inc., Toronto, Ontario, Canada) was used for simultaneous multi-elemental determination of major and minor elements. Sample preparation for ICP-AES analysis was as follows: Twenty milligrams of sample red clay was weighed precisely in Teflon digestion vessels, and 1 mL of a concentrated HNO_3 solution with 4 mL of an HF solution (Sigma-Aldrich, St Louis, Missouri, USA) was added. The samples were subjected to microwave heating for 75 min. After cooling, the colorless solutions were transferred quantitatively to 100 mL volumetric flasks and made up to volume with deionized water.

The oriented aggregate was used for study by XRD, and the < 2 mm fraction was separated using a Kubota Ks-8000 centrifuge (Tokyo, Japan). For the general study, an air-dried oriented aggregate was prepared by heating at 550°C for 4 h to destroy the kaolinite and confirm the absence of chlorite. The measurements were collected over the range 5 to 30°2θ with a step size of 0.02°2θ using CuKα (λ = 1.5405 Å).

Density is referred to as the median spatial distribution of mass in a material (Labbilta et al., 2021). The helium pycnometer is a practical density measurement tool for powders. In the helium pycnometer, the volume occupied by a defined powder mass is determined by measuring the volume of gaseous helium displaced by the powder. The ratio of mass to volume is the pycnometric density. The density determination was performed using a Micromeritics AccuPyc II 1345 instrument (Unterschleissheim, Germany). The value displayed is the average of 10 measurements.

The Bernard method is good for measuring rapidly the carbonate content percentage. The red clay was placed in a test tube connected to a graduated cylinder filled with water, and 10 ml of concentrated chloridric acid (1N) were added to 5 g of the clay powder (Sigma-Aldrich, St Louis, Missouri, USA). The CO_2 formed by the reaction pushed the water out of the graduated cylinder and was read directly on the scale. Therefore, the volume of gas released was measured and indicated the amount of carbonate contained in the sample.

Thermal analysis was used to track the mineral evolution and weight loss due to the release of adsorbed water, CO_2 (decarbonation reactions), and OH (dehydroxylation reactions) with increasing temperature. The thermal behavior was determined using a thermal analyzer (STA PT 1600, Linseis, Selb, Germany). Results were obtained under air from 25 to 1050°C at a heating rate of 10°C/min.

The thermal expansion and shrinkage of the compacted powder samples, pressed under 1 ton of pressure to obtain 13 × 5 mm pellets, was measured with a dilatometer (NETZSCH DIL 402 C, Selb, Germany) at a heating rate of 5°C/min between room temperature and 1050°C. The particle-size distribution of red clay was obtained using a Mastersizer 2000 laser size analyzer (Malvern Panalytical, Malvern, UK). The powder (~40 mg) was mixed with 40 mL of water, and the suspension was sonicated for 1 min to break the coarse agglomerates.

https://doi.org/10.1007/s42860-022-00208-2 Published online by Cambridge University Press

The physical properties of the samples after firing were investigated. The Archimedes method (Nor et al., 2008) measured the bulk density, apparent porosity, and water adsorption values for the fired samples. Ceramic samples were dried until the weight was unchanged (W_1). The samples were placed in a water tank for 24 h. The suspended weights of the samples in water were measured (W_2). The sample was then removed from the water, and the surface water was wiped off with a paper towel and weighed quickly (W_3). The water adsorption, apparent porosity, and apparent density values of the samples were calculated using the following three equations (El Ouahabi, 2013; Heah et al., 2013).

$$\text{Water Absorption } (\%) = \frac{W_3 - W_1}{W_1} \times 100 \quad (1)$$

$$\text{Apparent Porosity } (\%) = \frac{W_3 - W_1}{W_3 - W_2} \times 100 \quad (2)$$

$$\text{Apparent Density } (\%) = \frac{W_1}{W_1 - W_2} \times 100 \quad (3)$$

The microstructural morphology of the sintered ceramics was investigated using an Hitachi SC 2500 scanning electron microscope (Hitachi High-Technologies Corporation, Tokyo, Japan), with an acceleration voltage of 10 kV. In order to determine the shape of the red clay particles, the powder sample was dispersed fully in distilled water, homogenized ultrasonically, and deposited on the sample holder. The mechanical strength of the sintered red clay samples was evaluated by means of the 'Brazilian Test' (Ametek Lloyd instruments, Elancourt, France) (Rena et al., 2004). The load-displacement curves of the indirect tensile resistances were acquired at a load rate of 0.1 mm min^{-1}, and the pellet had dimensions of 13 mm × 5 mm.

Results and Discussion

Raw Material Analysis

Chemical, Elemental, and Mineralogical Analysis The chemical analysis, and mineralogical composition of red clay (Table 1) revealed that it consists mainly of silica (52.79%) and alumina (17.44%), present in significant quantities (> 70% of the total mass). In contrast, oxides of iron(III), potassium, calcium, magnesium, sodium, and phosphorus were present in small quantities (5.85%, 4.62%, 3.94%, 2.53%, 0.42%, and 0.17%, respectively).

The theoretical SiO_2/Al_2O_3 ratio associated with pure kaolinite is 1.18 (Heah et al., 2013; Tassongwa et al., 2014). Closer inspection of the XRF patterns herein showed that the SiO_2/Al_2O_3 ratio was > 3; this ratio indicates the relative amounts of clay minerals and quartz. A value >1.18 suggests an increased presence of free quartz.

The relatively large Fe_2O_3 and K_2O contents in red clay indicated that Fe and K are probably present in secondary minerals such as illite ($K_{0.5}(Al, Fe, Mg)_3(Si, Al)_4O_{10}(OH)_2$), as indicated by the XRD pattern of the untreated clay powder (Fig. 1). Other dominant phases were kaolinite ($Al_2Si_2O_5(OH)_4$) and quartz (SiO_2), with dolomite and calcite as carbonate phases. Elemental analysis of the raw materials (Table 1) revealed that red clay comprises mainly silicon, aluminum, iron, and potassium with small amounts of phosphorus and sodium (0.26–1.10 mg/L). These results are consistent with XRF analysis and mineralogical composition. An important conclusion is derived from the results given in Table 1, confirming that red clay is entirely free of heavy metals and radionuclides. This makes it usable as a raw material in ceramics, with no risks to human health. The relatively high value of loss on ignition (up to 11%) in red clay can be related to the

Table 1 Chemical analysis and mineralogical composition of red clay

Chemical composition (%)	CaO	SiO_2	P_2O_5	MgO	Al_2O_3	Fe_2O_3	K_2O	Na_2O	LOI%
	3.94	52.79	0.17	2.53	17.44	5.85	4.62	0.42	11.7
Elemental analysis (mg/L)	Ca	Si	P	Mg	Al	Fe	K	Na	
	8.88	98.30	0.26	3.92	33.52	17.57	14.45	1.10	
Mineralogical composition	Illite—Kaolinite—Dolomite—Quartz – Calcite								

https://doi.org/10.1007/s42860-022-00208-2 Published online by Cambridge University Press

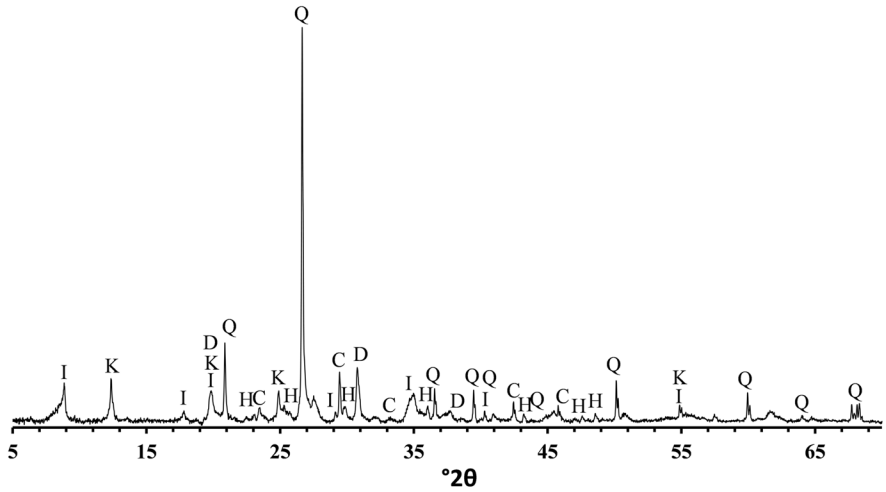

Fig. 1 XRD pattern of the raw clay powder. I: Illite, C: Calcite, K: Kaolinite, Q: Quartz, D: Dolomite, H: Hematite

significant presence of clay minerals and sometimes carbonates (dolomite-calcite).

The spectra of oriented aggregates (Fig. 2) confirmed the predominance of illite and kaolinite with no trace of any other clay mineral. The reflection of kaolinite disappeared on heating at 530°C for 4 h, while illite appeared throughout the heating treatment. These results agree with several previous studies (Carvalho, 2017; García & Camazano, 1968).

Thermal Analysis In the temperature range 25–1050°C, the variation trends in the TG curves of red clay were divided into two degradation stages (Fig. 3):

- The first stage was from ambient temperature to 150°C, with a weight loss of 1.82%, which is attributed to the removal of hygroscopic water (Marques et al., 2006).
- The second stage showed the most relevant weight loss (8.07%) within the range from 400 to 750°C, which could be divided into two steps: the first step (400–570°C) corresponds to the dehydroxylation reaction with a weight loss of 3.05%, and the second step (570–750°C) which might be attributable to the decomposition of calcite and magnesium carbonate, showing a weight loss of ~5.02% (Elias & Cultrone, 2019; Harech et al., 2019).

The DTA results of red clay revealed four endothermic peaks. A small endothermic peak at 95.0°C was attributed mainly to the removal of hygroscopic water. The stronger endothermic peak at 508°C could be attributed to the dehydroxylation of the kaolinite mineral following the temperature increase, which somewhat partially masks the dolomite decomposition peak at 568°C (Marques et al., 2006). Following the heating curve of DTA results, specifying the temperature of the allotropic transformation of quartz, was impossible. The cooling curve was drawn; following this representation, a small exothermic peak at 607°C corresponded to the conversion of β quartz to α quartz. Lastly, the exothermic peak observed at 900°C corresponded to the crystallization of new phases (anorthite-diopside). All these results are in accordance with the literature (Harech et al., 2021; Xie et al., 2016).

Thermal expansion must be considered when evaluating the potential applications of any material, especially when significant changes in dimension due to temperature are expected. Red clay showed a slight expansion of 0.15% between 20 and 90°C, followed by removing adsorbed water (0.25%) below 256°C (Fig. 4). At 700°C, the most significant expansion was observed, which was caused by structural change, probably by decomposition of carbonate (Pontikes et al., 2007). Due to sintering, further heating of clay between 800 and 940°C led to a gradual contraction of 5.2%. This finding is in accordance with clay

https://doi.org/10.1007/s42860-022-00208-2 Published online by Cambridge University Press

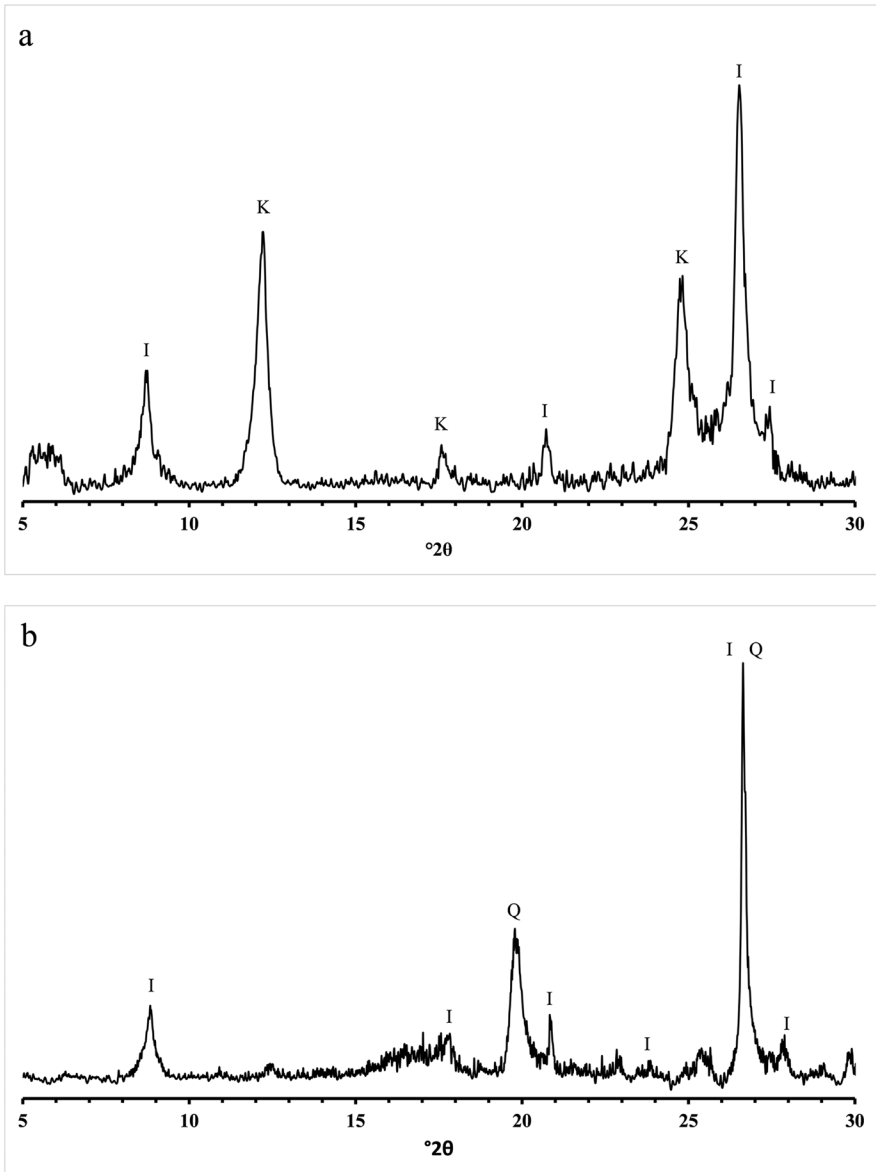

Fig. 2 XRD patterns of oriented aggregates: **a** normal oriented aggregates and **b** heated at 550°C

brick ASTM standards (Pontikes et al., 2007), which require a value of firing shrinkage of <8%. A slight shrinkage indicated the beginning of the melting phase with increasing temperature.

Particle-Size Distribution and Microstructure Analysis The particle-size distribution of red clay (Fig. 5 and Table 2) showed a bimodal distribution, with a range between 0.3 μm and 1 μm, and a major peak between 1.7 and 25.17 μm. According to these results, the average particle size of red clay is 6.32 μm, the sand percentage is 1.03%, silt 67.26%, and clay 31.7%. Furthermore, a restricted particle-size distribution was observed, which can help to expand the possible applications of this raw material, enabling the use of specific sizes by sieving or by the entire range of sizes. Also, the absence of a substantial proportion of sand makes sintering easier. This result is in line with the thermal expansion result. All these features make red clay a good choice for application in ceramics.

https://doi.org/10.1007/s42860-022-00208-2 Published online by Cambridge University Press

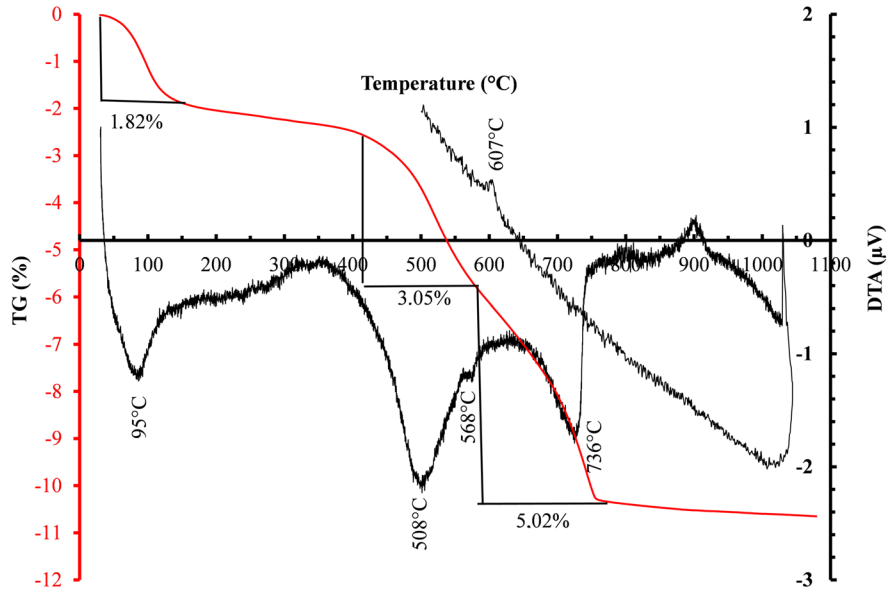

Fig. 3 DTA-TG curves of the red clay

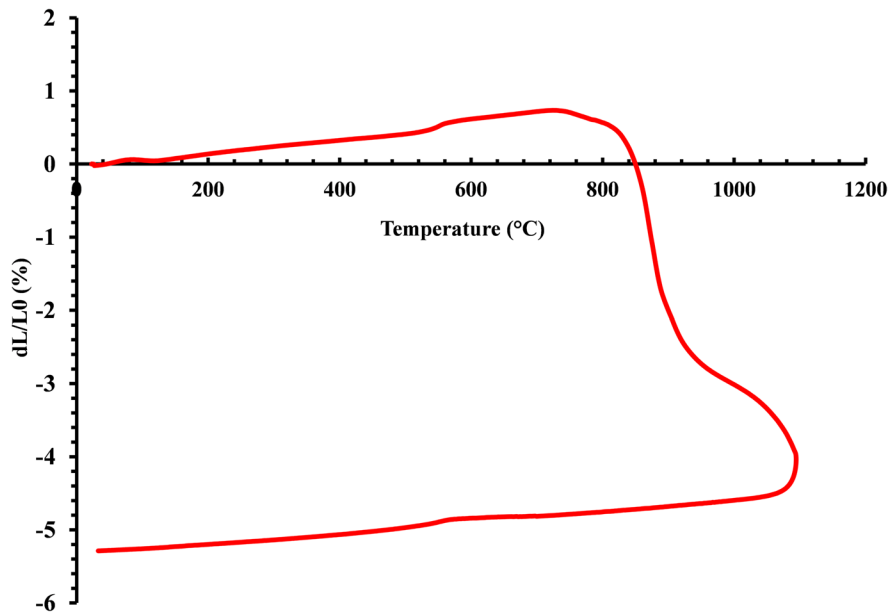

Fig. 4 Dilatometric curve of the red clay

Scanning electron microscopy of the clay powder revealed that it contains both spherical and irregular particle shapes (Fig. 6). The largest grains of the powder do not exceed 12 µm. The dispersion of the powder in distilled water by ultrasound prevented the agglomeration of the clay particles. At greater magnification, one of the largest grains was surrounded by very small particles, which are generally clayey phases.

Mineralogical Transformations Results from XRD analysis for fired red clay (Fig. 7) identified quartz, calcite, and illite as the main phases for the

https://doi.org/10.1007/s42860-022-00208-2 Published online by Cambridge University Press

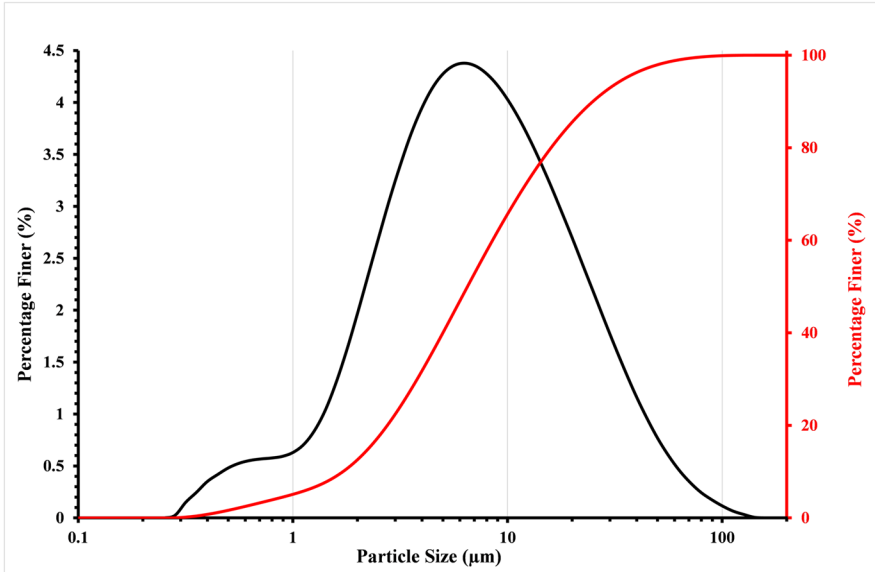

Fig. 5 Particle-size distribution of the red clay

Table 2 Particle-size distribution of red clay

Particle diameter (µm)	**D10**	1.7
	D50	6.32
	D90	25.17
Relative percentages of sand, silt, and clay (%)	Sand	1.03
	Silt	67.26
	Clay	31.7

D10: the corresponding particle size when the cumulative distribution percentage reaches 10%. **D50**: the corresponding particle size when the cumulative distribution percentage reaches 50%. **D90**: the corresponding particle size when the cumulative distribution percentage reaches 90%

sample fired at 600°C. The dolomite and kaolinite peaks were not detected. This is in line with the thermodynamic equilibrium system; by removing hydroxyl groups from the silicate lattice, kaolinite was decomposed into amorphous metakaolinite ($Al_2Si_2O_7$), while dolomite was decomposed into calcite and magnesium carbonate. Additional phases were probably formed but could not be determined because they were present in small quantities and their peaks on the XRD trace were unclear. The main phases detected at 900°C (Fig. 7) were anorthite ($CaAl_2Si_2O_8$) and diopside ($CaMgSi_2O_6$). Gehlenite ($Ca_2Al_2SiO_7$) appeared as an intermediate phase, and it became unstable when quartz or other SiO_2-based minerals were present and then reacted with the anorthite and wollastonite (Danner et al., 2018). The phase changes during the sintering of red clay between 600 and 1100°C are in good accord with the literature (Elias & Cultrone, 2019; Harech et al., 2022; Rathossi et al., 2004).

Density and the BET Surface Area The density and the BET surface area of red clay powders varied during heat treatment (Fig. 8). The density of clay corresponds to the density of its constituents. The density of clay powder increased from 2.67 to 2.92 g cm^{-3} after thermal treatment. All of the minerals detected by XRD for untreated red clay have a density between 2.61 and 2.66, except for calcite and dolomite, which are slightly denser. The small carbonate content measured by the Bernard-calcimetry method (indicating only 4% of carbonate) does not affect the density of the powder; that depends on the other minerals, which have density values close to that of the clay. After heat treatment at >900°C, diopside and anorthite were the main phases produced. The increase in density is related to the formation of these phases (diopside, anorthite), which are denser than the starting phases (Table 3). The evolution of the surface area of red clay after thermal treatment is shown in Fig. 8. With increasing temperature, the total internal surface area decreased from 37.80 to 27.24 m^2/g. The change was related to

https://doi.org/10.1007/s42860-022-00208-2 Published online by Cambridge University Press

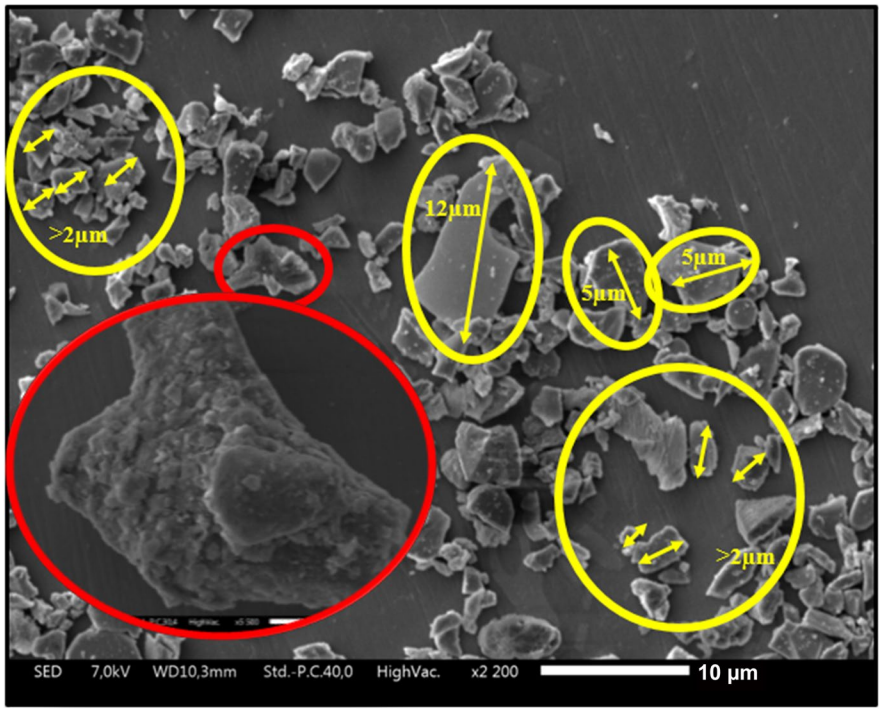

Fig. 6 SEM image of the red clay

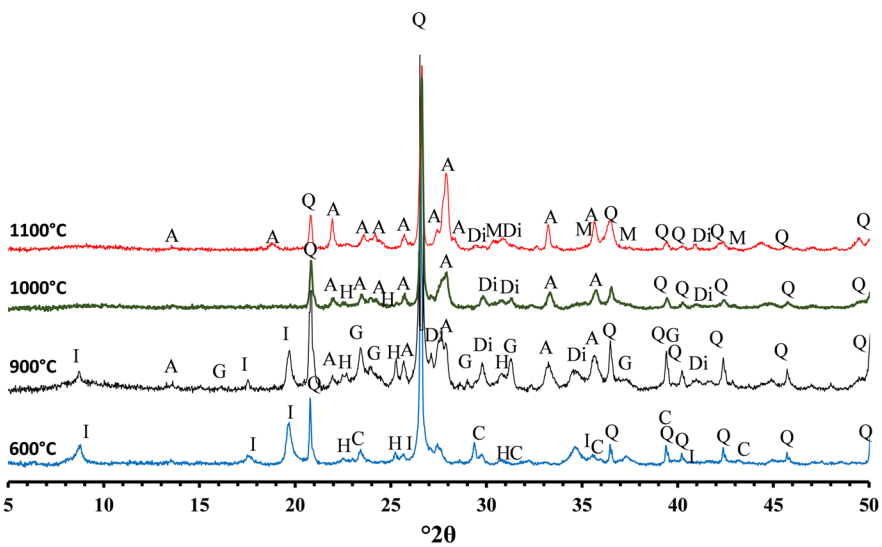

Fig. 7 XRD analysis of red clay fired at 600, 900, and 1100°C. I: Illite, C: Calcite, H: Hematite, Q: Quartz, Di: Diopside, A: Anorthite, M: Magnetite, G: Gehlenite

https://doi.org/10.1007/s42860-022-00208-2 Published online by Cambridge University Press

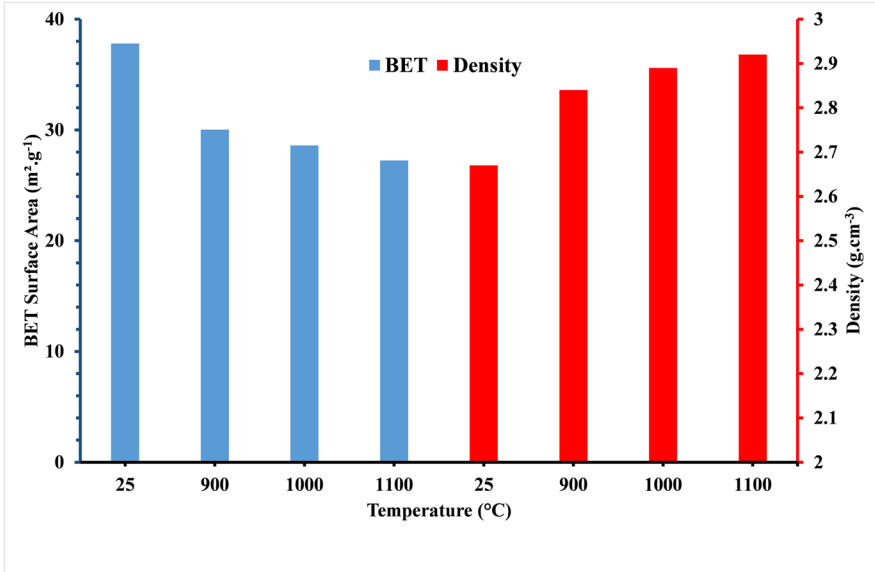

Fig. 8 Variation of density and the BET surface area of red clay powder

Table 3 Density of the minerals

Minerals	Quarts	Kaolinite	Illite	Dolomite	Calcite	Diopside	Anorthite	Gehlenite
Density (g/cm^3)	2.65	2.61	2.66	2.86	2.71	3.27	2.74–2.76	3.03–3.38
Ref	(Schulz & White, 1999)	(Nasser & James, 2006)	(Nasser & James, 2006)	(Barbhuiya, 2011)	(Teng, 2004)	(Stockmann et al., 2013)	(Agathopoulos et al., 2003)	(Bernardo et al., 2014; Kim & Kim, 2004)

the disappearance of the clay minerals, which consist of stacks of layers interspersed by interlamellar spaces; this influences significantly the BET surface area and the size of the grains, which increased due to sintering.

Fired Clay Analysis

Open Porosity and Density The mechanical and physical properties of the fired clay indicated that the red clay samples improved their firing properties over the temperature range 900–1100°C. The evolution of open porosity and water adsorption after firing at low and high temperatures is illustrated in Fig. 9. The smallest amount of water adsorbed was recorded for red clay fired at 1100°C (12.02%), while the maximum was obtained for the sample fired at 900°C (15.87%), showing that the open porosity decreased from 29.82% to 23.10% over this temperature interval, due to a closure of some of the pores.

The density was practically unchanged over the range 900–1100°C (2.76 and 2.85 g cm^{-3}, respectively) (Fig. 10). This is consistent with the density of sintered pellets at 900 and 1100°C, which could be explained by a change in closed porosity. Densification is a determining parameter that will affect the strength of ceramic products; it is caused by the formation of a glass phase (which fills the open porosity), and by the progressive formation of anorthite and diopside, which are phases that strengthen the material's mechanical properties (Domínguez-Ríos et al., 2009). The increase in temperature improved the mechanical properties of the materials and promoted the formation of solid phases (anorthite, diopside). This is confirmed by the XRD trace which showed an increase in anorthite peak reflections at 1100°C, and

https://doi.org/10.1007/s42860-022-00208-2 Published online by Cambridge University Press

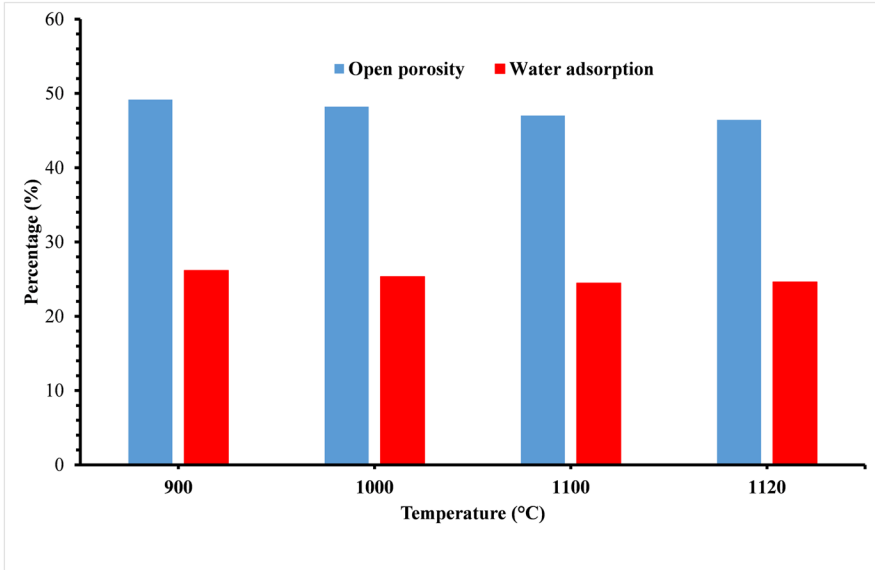

Fig. 9 Open porosity and water adsorption after firing at 900 and 1100°C

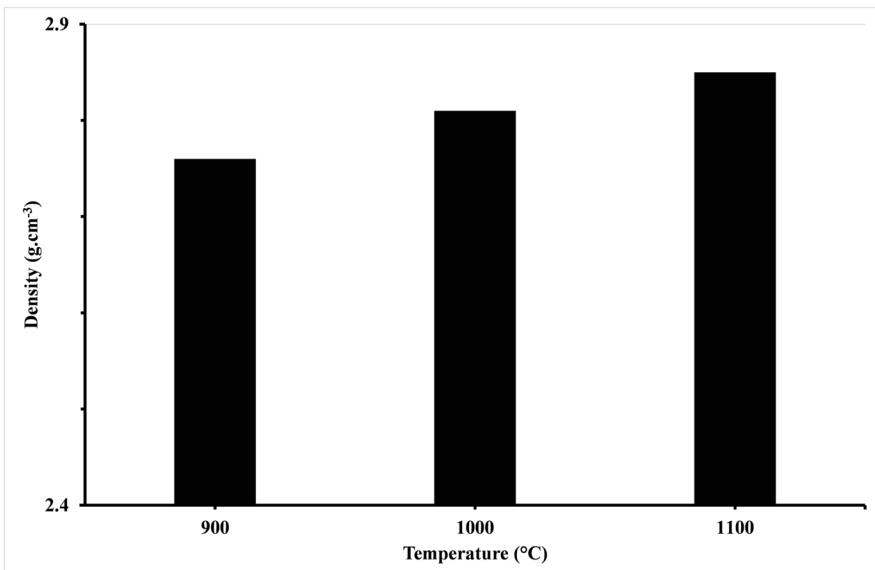

Fig. 10 Density of ceramic pellets sintered at 900, 1000, and 1100°C

by dilatometry, which showed the appearance of a glassy phase above 1100°C.

Morphological Analysis The large amount of alkalis and alkaline earths served as a flux and reduced the degree of porosity in ceramic products. This result was reinforced by the SEM images of ceramic materials fired at 900, 1000, and 1100°C (Fig. 11). The SEM image at 900°C illustrates perfectly the inhomogeneous microstructures and the presence of pores of various sizes. The high porosity is related to the dehydroxylation reaction and the carbonate decomposition, resulting in CO_2 release. At 1000 and 1100°C, the porosity decreased significantly after

https://doi.org/10.1007/s42860-022-00208-2 Published online by Cambridge University Press

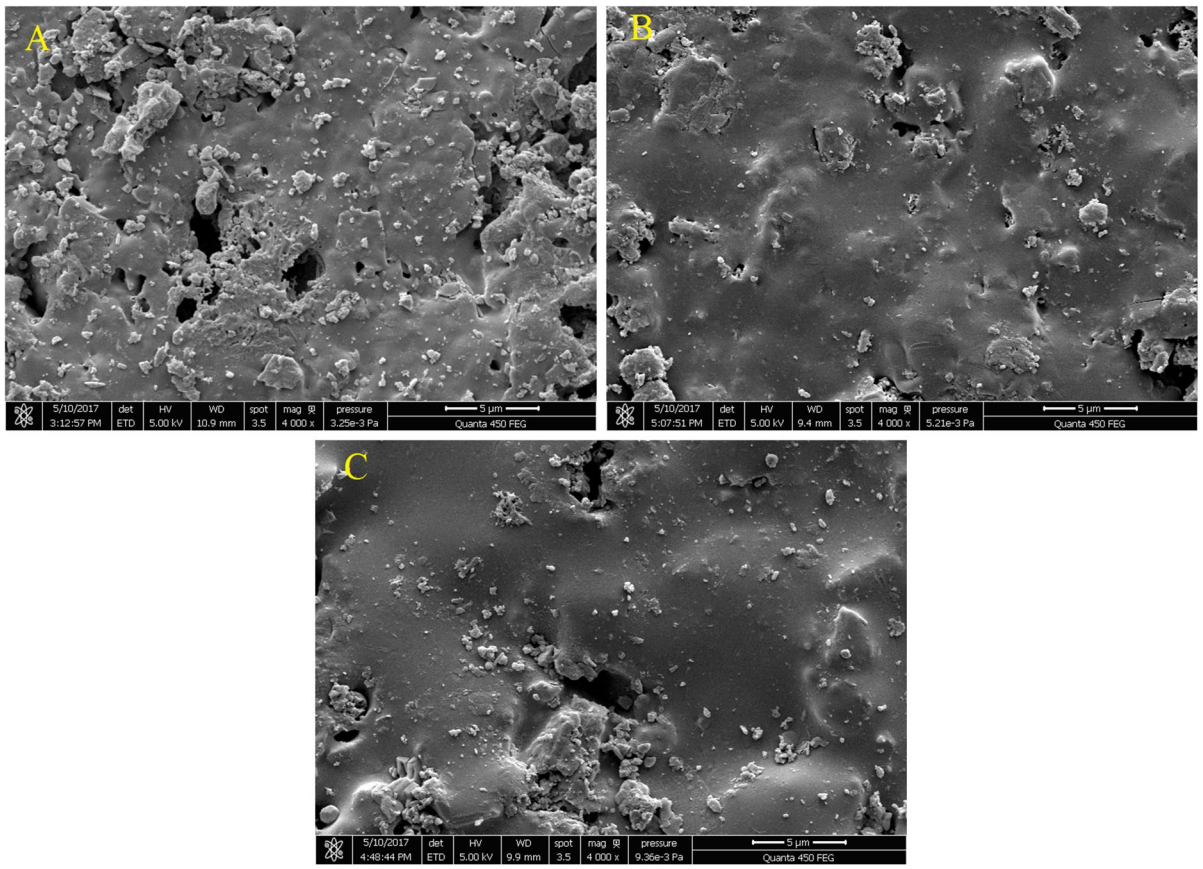

Fig. 11 SEM images of ceramic materials fired at: **A** 900, **B** 1000, and **C** 1100°C

vitrification. In accordance with the sintering process, the specimens exhibited a denser microstructure with poor porosity, which can be explained by the formation of the pore-filling glassy phase. In this case, the open porosity was limited, and closed spherical pores could be formed. The prevalence of an alkaline phase (K_2O, Na_2O) in the firing sample increased the vitrification process due to the flow effect of such oxides. The amount of amorphous silica released during the metakaolin decomposition may also lead to the formation of a glassy phase. The SEM images of the specimens showed that the bodies generally had low porosity, which might be explained by the small carbonate content.

Color Change The XRD pattern in Fig. 2 showed the presence of small amounts of free hematite. A study of the clay's color change after heat treatment was carried out to confirm this. The results indicated that the color of the clay after heat treatment became much redder, which means that a quantity of Fe_2O_3 was released. The XRD patterns (Fig. 7) showed that the intensity of Fe_2O_3 increased at 900°C before disappearing at 1100°C. This result is in good agreement with the mineralogical transformations because, after the decomposition of illite, an increase in the formation of anorthite and diopside from the Al_2O_3 and SiO_2 of the decomposed illite was observed. The Fe_2O_3 from this decomposition gave the clay this red color. At high temperatures, the pellet became dark due to the formation of Fe_3O_4 (Fig. 12).

Mechanical-Strength Analysis The mechanical strength of specimens according to the sintering temperature (Fig. 13) showed that the lowest tensile strength (324 N) was recorded at a sintering temperature of 900°C, while the highest value (918 N) was recorded at 1100°C, indicating a 283% increase. In

https://doi.org/10.1007/s42860-022-00208-2 Published online by Cambridge University Press

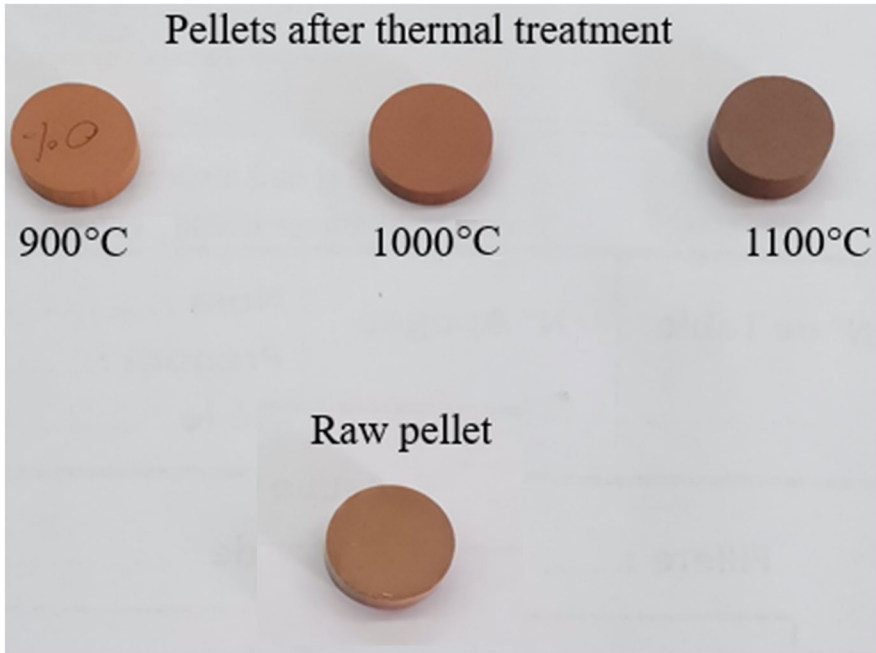

Fig. 12 Color changes in the pellets after thermal treatment

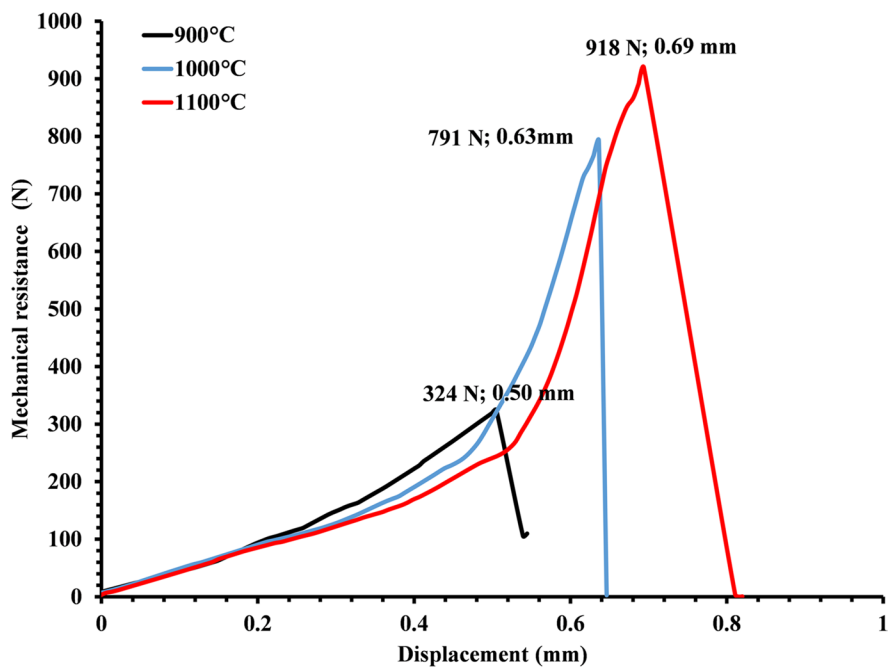

Fig. 13 Effect of sintering temperature on the indirect tensile strength of ceramics

https://doi.org/10.1007/s42860-022-00208-2 Published online by Cambridge University Press

these ceramics, the improvement of the tensile properties at the higher sintering temperature (1100°C) was attributed to the gradual formation of a glassy phase, which filled the tiny pores. This finding is in line with the SEM image, which showed a large, dense surface area with the complete absence of tiny pores. The formation of crystalline solid phases (diopside, anorthite) enhanced the mechanical strength. The samples sintered at 900°C showed a linear evolution with greater elasticity before failure, which was attributed to their excellent elasticity. However, the tensile load-displacement curves for the specimen sintered at 1100°C showed two different behaviors. The first was for the weak compression, where the material showed high plasticity, followed by a strong linear increase until sudden failure. This critical finding proved that the red clay material does not lose its elasticity even after high-temperature sintering.

Conclusions

The XRD pattern revealed that crystalline kaolinite and illite were the most abundant clay minerals in the raw red clay. The presence of kaolinite suggests that it could be used as a raw material in geopolymers. The changes in density and evolution of specific surface area are due to the mineralogical phases formed after heat treatment. The presence of anorthite is also a significant result, as it is widely known for its mechanical resistance and high performance in the vitroceramic field. The mechanical properties of ceramic pellets were improved significantly as the sintering temperature was increased from 900 to 1100°C. Raising the sintering temperature increased specimen density and mechanical strength and decreased open porosity and water adsorption. The mechanical strength increased by 283%, from 324 N (900°C) to 918 N (1100°C).

The physical and mechanical characteristics of red clay were analyzed here to obtain a clear impression of the technical quality of the raw material. This study has provided new data on the physicochemical changes in powdered red clay following thermal treatment. These data will be helpful in the manufacture of value-added ceramics.

Authors' Contributions All the authors contributed to the study's conception and design. Material preparation, data collection, and analysis were performed by Harech Mohamed Amine, Mesnaoui Mohamed, and Labbilta Tariq. Harech Mohamed Amine wrote the first draft of the manuscript, and all authors commented on previous versions. All authors read and approved the final manuscript.

Funding This research received no specific grants from any funding agency in the public, commercial, or not-for-profit sectors.

Data Availability All data are contained within the article.

Code Availability Not applicable.

Declarations

Conflict of Interest The authors declare that they have no conflict of interest.

References

Agathopoulos, S., Tulyaganov, D. U., Marques, P. A. A. P., Ferro, M. C., Fernandes, M. H. V., & Correia, R. N. (2003). The fluorapatite–anorthite system in biomedicine. *Biomaterials, 24*, 1317–1331.

Barbhuiya, S. (2011). Effects of fly ash and dolomite powder on the properties of self-compacting concrete. *Construction and Building Materials, 25*, 3301–3305.

Bernardo, E., Fiocco, L., Prnová, A., Klement, R., & Galusek, D. (2014). Gehlenite: Eu^{3+} phosphors from a silicone resin and nano-sized fillers. *Optical Materials, 36*, 1243–1249.

Carvalho, F. P. (2017). Mining industry and sustainable development: Time for change. *Food and Energy Security, 6*, 61–77.

Celik, H. (2010). Technological characterization and industrial application of two Turkish clays for the ceramic industry. *Applied Clay Science, 50*, 245–254.

Danner, T., Norden, G., & Justnes, H. (2018). Characterisation of calcined raw clays suitable as supplementary cementitious materials. *Applied Clay Science, 162*, 391–402.

Djangang, C. N., Elimbi, A., Melo, U. C., Lecomte, G. L., Nkoumbou, C., Soro, J., Bonnet, J. P., Blanchart, P., & Njopwouo, D. (2008). Sintering of clay-chamotte ceramic composites for refractory bricks. *Ceramics International, 34*, 1207–1213.

Domínguez-Ríos, C., Bocanegra-Bernal, M. H., & Aguilar-Elguézabal, A. (2009). Use of thermally treated bentonitic clay in the formulation of ceramic tiles. *Applied Clay Science, 46*, 271–276.

Elias, M. L., & Cultrone, G. (2019). On the use of sodium chloride and calcined diatomite sludge as additives to

improve the engineering properties of bricks made with a clay earth from Jun (Granada, Spain). *Minerals, 9*, 64.

El Ouahabi, M. (2013). *Valorisation industrielle et artisanale des argiles du Maroc* (pp. 86). PhD thesis, Univ. Liège, Liège, France.

García, S. G., & Camazano, M. S. (1968). Differentiation of kaolinite from chlorite by treatment with dimethyl-sulphoxide. *Clay Minerals, 7*, 447–450.

Harech, M. A., Mesnaoui, M., Abouliatim, Y., & El Hafiane, Y. (2019). *Evaluer l'effet de l'ajout d'argile sur les transformations minéralogiques de la boue de lavage de phosphate*. Limoges, France: PLUMEE.

Harech, M. A., Mesnaoui, M., Abouliatim, Y., Youssef, E. L., Benhammou, A., Abourriche, A., Smith, A., & Nibou, L. (2021). Effect of temperature and clay addition on the thermal behavior of phosphate sludge. *Boletín De La Sociedad Española De Cerámica y Vidrio, 60*, 194–204.

Harech, M. A., Dabbebi, R., Abouliatim, Y., Elhafiane, Y., Smith, A., Mesnaoui, M., Nibou, L., & Baklouti, S. (2022). A comparative study of the thermal behaviour of phosphate washing sludge from Tunisia and Morocco. *Journal of Thermal Analysis and Calorimetry, 147*(10), 5677–5686.

Heah, C. Y., Kamarudin, H., Bakri, M. A., & A. M., Bnhussain, M., Luqman, M., Khairul Nizar, I. & Liew, Y. M. (2013). Kaolin-based geopolymers with various NaOH concentrations. *International Journal of Minerals, Metallurgy, and Materials, 20*, 313–322.

Jordan, M. M., Montero, M. A., Meseguer, S., & Sanfeliu, T. (2008). Influence of firing temperature and mineralogical composition on bending strength and porosity of ceramic tile bodies. *Applied Clay Science, 42*, 266–271.

Kabre, T. S., Traore, K., & Blanchart, P. (1998). Mineralogy of clay raw material from Burkina Faso and Niger used for ceramic wares. *Applied Clay Science, 12*, 463–477.

Kim, J. M., & Kim, H. S. (2004). Glass-ceramic produced from a municipal waste incinerator fly ash with high Cl content. *Journal of the European Ceramic Society, 24*, 2373–2382.

Labbilta, T., Ait-El-Mokhtar, M., Abouliatim, Y., Khouloud, M., Meddich, A., & Mesnaoui, M. (2021). Elaboration and Characterization of Vitreous Fertilizers and Study of Their Impact on the Growth, Photosynthesis and Yield of Wheat (Triticum durum L.). *Materials, 14*, 1295.

Marques, V. M. F., Tulyaganov, D. U., Agathopoulos, S., Gataullin, V. K., Kothiyal, G. P., & Ferreira, J. M. F. (2006). Low temperature synthesis of anorthite based glass-ceramics via sintering and crystallization of glass-powder compacts. *Journal of the European Ceramic Society, 26*, 2503–2510.

Monteiro, S. N., & Vieira, C. M. F. (2004). Solid state sintering of red ceramics at lower temperatures. *Ceramics International, 30*, 381–387.

Nasser, M. S., & James, A. E. (2006). The effect of polyacrylamide charge density and molecular weight on the flocculation and sedimentation behaviour of kaolinite suspensions. *Separation and Purification Technology, 52*, 241–252.

Njoya, D., Hajjaji, M., & Njopwouo, D. (2012). Effects of some processing factors on technical properties of a clay-based ceramic material. *Applied Clay Science, 65*, 106–113.

Nor, M. A. A. M., Hong, L. C., Ahmad, Z. A., & Akil, H. M. (2008). Preparation and characterization of ceramic foam produced via polymeric foam replication method. *Journal of Materials Processing Technology, 207*(1–3), 235–239.

Pontikes, Y., Nikolopoulos, P., & Angelopoulos, G. N. (2007). Thermal behaviour of clay mixtures with bauxite residue for the production of heavy-clay ceramics. *Journal of the European Ceramic Society, 27*, 1645–1649.

Rathossi, C., Tsolis-Katagas, P., & Katagas, C. (2004). Technology and composition of Roman pottery in northwestern Peloponnese, Greece. *Applied Clay Science, 24*, 313–326.

Rena, C. Y., Ruiz, G., & Pandolfi, A. (2004). Numerical investigation on the dynamic behavior of advanced ceramics. *Engineering Fracture Mechanics, 71*(4–6), 897–911.

Schulz, M. S., & White, A. F. (1999). Chemical weathering in a tropical watershed, Luquillo Mountains, Puerto Rico III: Quartz dissolution rates. *Geochimica et Cosmochimica Acta, 63*, 337–350.

Stockmann, G. J., Wolff-Boenisch, D., Gislason, S. R., & Oelkers, E. H. (2013). Do carbonate precipitates affect dissolution kinetics?: 2: Diopside. *Chemical Geology, 337*, 56–66.

Strazzera, B., Dondi, M., & Marsigli, M. (1997). Composition and ceramic properties of tertiary clays from southern Sardinia (Italy). *Applied Clay Science, 12*, 247–266.

Tassongwa, B., Nkoumbou, C., Njoya, D., Njoya, A., Tchop, J. L., Yvon, J., & Njopwouo, D. (2014). Geochemical and mineralogical characteristics of the Mayouom kaolin deposit, west Cameroon. *Earth Science Research, 3*, 94.

Teng, H. H. (2004). Controls by saturation state on etch pit formation during calcite dissolution. *Geochimica et Cosmochimica Acta, 68*, 253–262.

Xie, J., Chen, T., Xing, B., Liu, H., Xie, Q., Li, H., & Wu, Y. (2016). The thermochemical activity of dolomite occurred in dolomite–palygorskite. *Applied Clay Science, 119*, 42–48.